Photochemistry of Fe:H2O Adducts in Argon Matrixes: A Combined Experimental and Theoretical Study in the Mid-IR and UV–Visible Regions

Vincent Deguin, Joëlle Mascetti, Aude Simon, Nadia Ben Amor, Christian Aupetit, Sandra Latournerie, Jennifer A. Noble

Photochemistry of Fe:H_2O Adducts in Argon Matrices: a Combined Experimental and Theoretical Study in the mid-IR and UV-visible Regions

Vincent Deguin,[†] Joëlle Mascetti,[†] Aude Simon,[‡] Nadia Ben Amor,[‡] Christian Aupetit,[†] Sandra Latournerie,[†] and Jennifer A. Noble[*,¶,§]

Institut des Sciences Moléculaires (ISM), Université de Bordeaux and CNRS, 351 Cours de la Libération, F-33405 Talence, France., Univ. Toulouse UPS CNRS, Lab. Chim. & Phys. Quant. LCPQ IRSAMC, 118 Route Narbonne, F-31062 Toulouse, France., and Univ. Lille 1, Lab. Phys. Lasers Atomes & Mol., CNRS, UMR 8523, F-59655 Villeneuve D'Ascq, France.

E-mail: jennifer.noble@univ-lille1.fr
Phone: +33 (0)3 20 43 49 87. Fax: +33 (0)3 20 43 40 84

Abstract

The photochemistry of Fe:H_2O adducts is of interest in fields as diverse as catalysis and astrochemistry. Industrially, iron can be used as a catalyst to convert H_2O to H_2, while in the interstellar medium it may be an important component of dust grains, influencing the chemistry on their icy surfaces. This study consisted of the deposition and spectral characterisation of binary systems of atomic iron with H_2O in cryogenic argon matrices. In this way, we were able to obtain information about the interaction of the two species; we observed the formation of adducts of iron monomers and dimers with water molecules in the mid-IR and UV-visible spectral domains. Upon irradiation with a UV radiation source, the iron species were inserted into the water molecules to form HFeOH and HFe_2OH, leading in some cases to the formation of FeO possibly accompanied by the production of H_2. DFT and correlated multireference wave function calculations confirmed our attributions. This combination of IR and UV-visible spectroscopy with theoretical calculations allowed us to determine, for the first time, the spectral characteristics of iron adducts and their photoproducts in the UV-visible and in the OH stretching region of the mid-IR domain.

Introduction

Iron atoms can form adducts with water, which rearrange upon UV irradiation to form insertion molecules. Such Fe_n:H_2O_m adducts and their photoproducts are of interest in diverse fields of research, including catalysis, atmospheric chemistry, corrosion, and astrochemistry. The use of transition metals as catalysts has been an active area of research since the en-

[*]To whom correspondence should be addressed

[†]Institut des Sciences Moléculaires (ISM), Université de Bordeaux and CNRS, 351 Cours de la Libération, F-33405 Talence, France.

[‡]Univ. Toulouse UPS CNRS, Lab. Chim. & Phys. Quant. LCPQ IRSAMC, 118 Route Narbonne, F-31062 Toulouse, France.

[¶]Univ. Lille 1, Lab. Phys. Lasers Atomes & Mol., CNRS, UMR 8523, F-59655 Villeneuve D'Ascq, France.

[§]Previous address: Institut des Sciences Moléculaires (ISM), Université de Bordeaux and CNRS, 351 Cours de la Libération, F-33405 Talence, France.

ergy crisis of the 1960s, with the production of H_2 from H_2O of particular interest.[1] Iron:water adducts are also important in the Earth's upper atmosphere, where a layer of iron atoms is present in the mesosphere due to meteoritic ablation. Fe is efficiently scavenged from the metallic layer by water-ice particles upon the formation of polar mesospheric clouds, and thus Fe interaction with water is key to the reactivity in these clouds.[2] The astrophysical relevance of Fe:H_2O interactions is due to the depletion of gas phase Fe in dense interstellar regions at rates higher than 90 %, which is believed to be predominantly due to the presence of Fe in its metallic form in the solid phase.[3] Where this iron is incorporated into icy dust grains, energetic processing by cosmic rays or photons could give rise to oxygenated iron species.

Such a wide range of applications has led to much fundamental experimental and theoretical investigation of the activation of water by iron clusters. Many studies are performed on cationic species, due to the ease of implementation (both experimentally and theoretically).[4–10] In particular, groups have studied IR signatures,[7,9,10] photofragmentation,[6] or mass spectra[4,5,8,10] and performed density functional theory (DFT) calculations[9,10] on Fe^+:H_2O_n complexes. Water dissociation was observed in a few cases.[10] Investigations of the reactivity of neutral iron atoms/clusters with water molecules are scarcer.[11,12] Water dissociation has also been observed on neutral iron clusters,[1,13] as well as on iron surfaces.[14–17] In order to mimic the cold, low pressure conditions of the Earth's upper atmosphere or astrophysical environments, experiments must be carried out in a cryogenic set-up, using spectroscopic diagnostics to observe the iron:water adducts and their reaction products. Vibrational spectroscopy has previously been used to study Fe:H_2O adducts and their photoproducts in argon matrices[11] in the context of a wider study of the interaction of transition metals with water. The subject was more recently revisited in a joint theoretical and experimental study using DFT to explore the potential energy surface (PES) of the observed photoreactions.[12] While both previous studies were carried out on neutral Fe in argon matrices, the more recent work by Zhang *et al.*[12] produced Fe atoms using laser evaporation, rather than the heating resistance method employed by Kauffman *et al.*[11] Laser evaporation often produces metal atoms in electronically excited states, rather than the ground state, which could impact the subsequent UV-induced photolysis studies. Importantly, neither of the previous photochemical studies addressed the ν_1/ν_3 OH stretching bands in the mid-IR or considered the UV-visible spectra of these complexes.

Quantum calculations on unsaturated clusters including transition metals are challenging due to both the complexity of the PES for such clusters, and to their open shell character. Pure theoretical work on the structures and energetics of $Fe_nH_2O^{+/0/-}$ (n=1-4) clusters, computed at the DFT level with the BPW91 functional,[18,19] was published by Gutsev *et al.*[20] For a given stoichiometry, several isomers were optimised and for each isomeric structure, several spin-states were considered. The authors then focused on the most stable structure for a given stoichiometry and computed its harmonic vibrational frequencies. Zhang *et al.*[12] also computed the harmonic spectra of the Fe:H_2O adducts and their (presumed) photoproducts. This was done with the B3LYP functional, which considerably overestimates the energy of the stretching water modes. Regarding the reaction paths, the mechanism for the reaction of Fe with H_2O was investigated by means of DFT and wave function correlated methods.[21] This study by Karlicky and Otyepka[21] demonstrates that DFT approaches fail to accurately reproduce the PES, making the use of correlated wave function approaches such as Coupled Cluster Single, Double and perturbative Triple CCSD(T) mandatory for Fe:H_2O systems. DFT studies have also been performed with the B3LYP functional to investigate the energetics of the reaction of metal dimers, among them Fe_2, with water.[1]

To the best of our knowledge, no UV-visible spectroscopy of Fe:H_2O and its HFeOH photoproduct has been published. This is likely due in part to the time consuming and challeng-

ing nature of the calculations required in order to allow the identification of the experimental bands. Owing to the multireference character of the states, multireference methods are required to obtain the most accurate electronic spectra, as previously shown for $[Fe(C_6H_6)]^+$.[22] In addition very large basis sets and a large active space must be used. Due to the degeneracies, the calculations have been done for a very large number of states. In this study we could not have performed the same type of calculation for complexes containing two iron atoms with equivalent active space.

We present a joint experimental and theoretical study of Fe:H_2O adducts and their UV photoproducts, extending previous experimental and theoretical studies to cover the ν_1/ν_3 OH stretching bands in the mid-IR and the UV-visible spectra of these species. To the best of our knowledge this represents the first joint UV-visible spectroscopic study of Fe:H_2O and its photoproducts. The ν_1/ν_3 OH stretching region and the UV-visible region are of particular interest in astrophysical studies, where these spectral regions are important probes of the chemical and physical nature of interstellar environments including star forming regions.

Experimental and theoretical methods

Experiments were performed in a high vacuum experimental setup consisting of a stainless steel chamber (base pressure 10^{-7} mbar) containing a CsBr substrate cooled to 10 K by a closed-cycle He cryostat. Deionised water was subjected to multiple freeze-pump-thaw cycles under vacuum to remove dissolved gases. Argon and water were mixed in a dosing line (at varying concentrations) and dosed into the chamber at a rate of 2 ml min^{-1}. Simultaneously, iron atoms were sublimated from an iron filament (38 mm × 10 mm × 0.5 mm, Goodfellow, 99.99 %) by application of a voltage of ∼ 1.3 V. Depositions lasted approximately two hours. Additional experiments were performed using deuterated water (Eurisotop 99.9 %) to aid attributions. Infrared spectra were obtained in transmission mode using a Bruker 70 V Fourier Transform InfraRed (FTIR) spectrometer with a DTGS mid-IR detector. Spectra were recorded from 4000 – 400 cm^{-1} at a resolution of 0.5 cm^{-1} and an average of ∼ 100 scans. UV-visible spectra were obtained in transmission mode using a Shimadzu UV 2600 UV-visible spectrometer. Spectra were recorded from 200 – 600 nm at a resolution of 0.2 nm. The deposited Fe:H_2O:Ar matrices were annealed to 20–25 K, recooled to 10 K, then irradiated with a mercury lamp for three minutes ($\lambda < 235$ nm, average power ∼ 150 mW). All spectra were measured at 10 K.

In order to rationalise the experimental results, quantum chemical calculations were performed using two levels of theory, based on *i)* DFT for structure determination and the production of IR spectra, and on *ii)* multireference wave function approaches for the determination of electronic spectra. The geometries of $Fe_xH_yO_z$ complexes (with x, y and z values between 0 and 2) likely to be formed in our matrix experiments were optimised with the gradient corrected BPW91 functional, a combination of Becke's exchange[18] and Perdew-Wang's correlation functional,[19] in conjunction with the triple-ζ cc-pVTZ basis set. In the discussion below, we will occasionally refer to the BPW91/cc-pVTZ level as "DFT" for the sake of simplicity. For $Fe_xH_yO_z$ and their deuterated counterparts, the harmonic IR spectra were obtained after full diagonalisation of the weighted Hessian matrix. It is worthwhile noting that the vibrational frequencies reported here are not scaled. The BPW91 functional was chosen as it was shown to provide the best results when comparing harmonic frequencies of Fe_2CO (and Co_2CO) complexes with those measured in matrix (10 – 60 cm^{-1} discrepancies).[23,24] In these papers, unscaled DFT harmonic spectra of isolated complexes are compared to rare gas matrix results and the agreement is very satisfactory. We therefore decided to use the same approach, and in particular not to take into account for some anharmonic effect using scaling factors. In this way, we do not biase the calculations. Indeed, scaling factors are very

likely to be mode dependent, and anharmonic effects are expected to be different for hydrogenated and deuterated species. Besides, we do not describe matrix effects in the calculations, and these may also be important to take into account if we want to compute accurate IR spectra. This functional was also used by Gutsev *et al.*[20] to perform an exhaustive exploration of the PES of $Fe_{1-4}(H_2O)^{1/0/+}$ complexes. As mentioned above, the authors of that study only focused on the most stable isomers for a given stoichiometry, and some of these were found to be irrelevant to our study, *i.e.* impossible to form under the experimental conditions used here. On the other hand, some species which were deemed by Gutsev *et al.*[20] to be likely to form in the present experiments were not identified in our matrices. We also specify that we used some of their results as starting point calculations in the appropriate cases. Indeed, their work was very useful in helping determine some of the most stable structures and spin-states in the present work. The BPW91 functional has, however, proven to provide a poor description of the energetics for several intermediates of the reaction of water with Fe in CCSD(T) calculations,[21] showing an overall overestimation of Fe-O binding energies. Therefore, in order to obtain energetic data on water:iron adducts, single point CCSD(T)/cc-pVTZ//BPW91/cc-pVTZ calculations, occasionally referred to as "CCSD(T)//DFT" below, for the sake of simplicity, were also performed. For iron:water molecular complexes – with non covalent (weak) metal-ligand interactions – the role of dispersion interactions may be non-negligible, and these are not taken into account in the BPW91 potential. Therefore we investigated the influence of dispersion by adding the D2 version of Grimme's dispersion[25] to the BPW91 potential. The geometries of the molecular complexes were then re-optimised and the harmonic IR spectrum re-computed using this BPW91-D2 potential.* Such an approach has been recently used to study vanadium-water complexes.[26] The BPW91-D2 approach will be labelled "DFT-D" for the sake of simplicity. The Gaussian09 suite of programmes[27] was used for both DFT and CCSD(T) calculations. Regarding convergence criteria, a tight convergence criterion was used for SCF cycles, *i.e.* 10^{-8} for the root mean square (RMS) change, in conjunction with a maximum change of 10^{-6} in the density matrix. In the case of SCF convergence problems, a Fermi temperature and (sometimes) a quadratic convergence algorithm were required. A very tight convergence criterion was used for geometry optimisation *i.e.* 10^{-6} for the RMS force, in conjunction with an ultrafine integration grid.

Concerning the electronic spectra, the calculations of the different states were carried out with the 7.8 MOLCAS package[28–30] and were based on Relativistic Correlation Consistent Atomic Natural Orbitals (ANO-RCC)[31,32] basis sets. For Fe, a (21s15p10d6f4g2h) basis set was contracted to [7s6p4d3f2g1h]; for O a (14s9p4d3f2g) set was contracted to [5s4p3d2f1g] and for H a (8s4p3d1f) set was contracted to [6s4p3d1f]. Scalar relativistic effects were taken into account by using the second-order Douglas-Kroll-Hess Hamiltonian.[33,34] C_1 spatial symmetry was used for Fe, Fe:OH_2 and HFeOH calculations. The zeroth-order description was obtained by means of complete active space self-consistent field (CASSCF) calculations.[35] For the iron atom and the Fe:OH_2 complex, the active space consists of the 3d, 4s, 4p and five correlating 3d' orbitals, leading to eight electrons in 14 orbitals, and is denoted CAS(8,14). This active space allows the description of the ground state – $^5D_4(3d^64s^2)$ for the iron atom; ^{5}A" for Fe:OH_2 ($3d^64s^2$) – as well as of all the quintet excited states until 240 nm, corresponding to the lowest wave-numbers observed in the experimental study. The number of calculated quintet states takes into account the number of degenerate components of the considered states. In the case of the iron atom, in order to get all these states, it was necessary to calculate 103 quintet

*We specify here that we used a value of 1.2 for s_6 in Equation (11) of Grimme *et al.*[25] To be completely accurate, the value of such a coefficient should be determined specifically for the BPW91 functional, but this is beyond the scope of the current study.

states corresponding to the ^{5}D ($3d^64s^2$), ^{5}F, ^{5}P ($3d^74s^1$), ^{5}D, ^{5}F, ^{5}P, ^{5}S, ^{5}G, ^{5}I, ^{5}H ($3d^64s^14p^1$), ^{5}D, ^{5}F, and ^{5}G ($3d^74p^1$) configurations. For the Fe:OH_2 complex, 70 quintet states have been calculated. Concerning the HFeOH complex, the active space consists of the 3d, 4s, one 4p (in-plane $4p_x$, perpendicular to the y axis of the molecule) and five correlating 3d' orbitals for the iron, of one occupied orbital involving the oxygen atom and its two neighbours, *i.e.* the hydrogen and the iron, and of one orbital for the terminal hydrogen atom, leading to 10 electrons in 14 orbitals, and is denoted CAS(10,14). To reach the upper part of the spectrum (200 nm), 30 quintet states were calculated. The ground state for the HFeOH complex is ^{5}A" $H^-Fe^{2+}(3d^6)O^-H$ with a NBO (Natural Bond Orbital) population of H($1s^{1.59}$)-Fe($4s^{0.37}3d^{6.07}4p^{0.18}$)-O($2s^{1.79}2p^{5.46}$)-H($1s^{1.59}$).

In addition to the CASSCF wave function, dynamical polarisation and correlation effects were then included following the Complete Active Space with Perturbation at the Second Order (CASPT2)[36] or Multi State CASPT2 (MS-CASPT2).[37] All the electrons are correlated. The Cholesky decomposition technique,[38,39] which allows a drastic reduction of the number of bielectronic integrals, was used with a 10^{-8} a.u. threshold. Spin-orbit coupling was calculated as the state interaction between the spin orbit free states by the restricted active space state interaction approach (SO-RASSI).[40] Concerning the iron atom, a small splitting (the mean value for the 103 roots is about 60 cm^{-1}) of the degenerate states appears at the CASPT2 level. The degeneracy is re-established by averaging the 2J+1 CASPT2 energies of the components of a given J. These energies and CASSCF wavefunctions are considered in the SO-RASSI calculations.[41] This procedure only leads to tiny differences in the final energy levels compared to the MS-CASPT2 SO-RASSI, but allows an accurate assignment of the SO states. However, for the Fe:OH_2 and HFeOH complexes, both wave functions and energies are those of the MS-CASPT2 calculations. In none of the electronic spectra calculated here was the argon matrix included. To avoid intruder states, the real level shift was applied in all the CASPT2 calculations, with a value of 0.4 a.u.. The Ionisation Potential-Electron Affinity (IPEA) shift[42] was not used here as there is some controversy in the literature concerning its application.[43–51] The validation of the different CASPT2 parameters was performed by determining the $^5D_4$-$^5F_5$ energy splitting of the iron atom with different IPEA and level shifts. For this, 12 states were calculated, corresponding to the ^{5}D ($3d^64s^2$) and ^{5}F ($3d^74s^1$) configurations. A full discussion is presented in the SI, including Table S1.

Results and discussion

Fe and Fe adducts with H_2O

Four experimental depositions of Fe:H_2O:Ar were made with varying H_2O concentrations. The spectra of these matrices are presented in Figures 1 and 2. In both of these figures, trace a is a H_2O:Ar reference spectrum, and traces b–e are Fe:H_2O:Ar matrices of increasing H_2O concentration. The attribution of experimental IR and UV-visible absorption bands is presented in Tables 1 and 2, respectively, based upon comparison with quantum chemical calculations.

In the Fe:H_2O:Ar matrix with the lowest H_2O concentration (trace b, Figures 1 and 2), only a small trace amount of H_2O is present, due to the low level contamination of the experimental chamber with H_2O. When the iron filament is heated, water molecules adsorbed to nearby metal surfaces desorb into the gas phase and are deposited along with the iron in the matrix. As the concentration of H_2O in the matrix increases, by mixing of water with the matricial gas, argon, the water molecules are present in aggregates of larger sizes. The characterisation of water aggregates in our experimental setup has been done previously in a combined experimental and theoretical study.[58] In the present study, we observe only water monomers and dimers in trace c (Figures 1 and 2), with larger aggregates (up to the hexamer) observed for traces d and e (Figures 1 and 2).

In all four Fe:H_2O:Ar matrices, iron has approximately a constant concentration, and is

present in both monomeric and dimeric forms. This is confirmed by the presence of multiple bands corresponding to Fe and Fe_2 in the UV-visible spectrum (Figure 2, right hand panel, and Table 2). In the present work, we produce Fe atoms using resistive heating, as in the study of Kauffman *et al.*,[11] to ensure that all Fe atoms are in the ground electronic state. This would not necessarily be the case for Fe atoms produced by laser ablation methods, as in the study of Zhang *et al.*[12] Attribution of Fe bands in the UV spectra were made by comparison with literature values for free Fe atoms[55] and Fe in an argon matrix at 4.2 K,[56] as well as by comparison with the calculated electronic spectrum.

For the electronic spectrum of atomic iron, the 103 calculated quintet states were identified in the following order: a^5D a^5F a^5P z^5D z^5F z^5P y^5D y^5F y^5P z^5G y^5G z^5S x^5D x^5P z^5H z^5I x^5F. Including the spin-orbit coupling gives rise to 515 spin-orbit states. Spin-orbit states with an oscillator strength higher than 0.01 (relative value, defined with respect to the maximum of 0.041) are presented in Table 2, with the corresponding energies and oscillator strengths.

The most intense band corresponds to a transition to the y^5D_4 state. Compared to experimental results[55] the agreement is rather good, in the range from -9 to 9 nm (-1540 cm^{-1} to 690 cm^{-1}), except for the highest x^5F_5 state for which the error is 16 nm (2830 cm^{-1}), which is the largest one. All the calculated states are presented in Table S2 in the SI. The theoretical work proposes three missing values in the experimental data, corresponding to the three quintet states z^5I_8, z^5I_7 and z^5H_7. The oscillator strengths are not comparable to the experimental intensities and can not been used for the assignment. The $^5D_4$-$^5F_5$ energy splitting of 1.16 eV (9320 cm^{-1}) is shifted by 0.16 eV compared to the value obtained for 12 roots (Tables S1 and S2 in the SI). Averaging the orbitals on 103 roots introduces a bias which is quite unavoidable. However, this calibration gives some hints on the accuracy expected for the two complexes for which smallest number of states are investigated (70 for $Fe:OH_2$ and 30 for HFeOH). Better agreement is found for the energy splitting of the $^5D_4$-$^5F_5$ states of the iron atom with the Multireference Configuration Interaction method (MRCI),[59] with the minimal eight electrons in six orbitals active space necessary to describe the $3d^64s^2$ and $3d^74s^1$ configurations. To also describe the $3d^64s^14p^1$ and $3d^74p^1$ states, a larger active space which includes the 4p orbitals is necessary and the MRCI method is no longer adapted. The CASPT2/MS-CASPT2 method used in this study is a good compromise between the feasibility of the calculation and the accuracy of the results. Finally, the presence of the argon matrix gives rise to a slight blueshift compared to the free atom and it is expected that the same shift occurs in the two complexes.

Deposition of Fe with H_2O produced $Fe:H_2O$ and $Fe_2:H_2O$ adducts in the argon matrices. In the ν_2 OH bending mode region, absorption bands are observed at 1562 cm^{-1} and 1579 cm^{-1}, corresponding to $Fe:H_2O$ and $Fe_2:H_2O$, respectively (see Figure 1, left-hand panel, and Table 1). These modes were shifted to 1159 and 1169 cm^{-1}, respectively, in experiments with deuterated water (see Table 3). This is in agreement with the previous experimental studies of Kauffman *et al.*[11] and Zhang *et al.*[12] The attributions of the complexes (including those with D_2O) are confirmed by our DFT calculations (Table 1), as discussed in detail below. At low frequencies we see no absorption bands corresponding to Fe-related adducts or molecules upon deposition (see Figure 1, right-hand panel). This is in agreement with the study of Kauffman *et al.*,[11] where Fe was deposited thermally, as in our current work. There is no evidence of the deposition of FeO, unlike the study of Zhang *et al.*,[12] where Fe was deposited by laser ablation.

The spectral properties of the adducts $Fe:H_2O$ and $Fe_2:H_2O$ have not previously been published in the ν_3/ν_1 OH stretching region or in the UV-visible region. In the ν_3/ν_1 OH stretching region, we observe absorption bands at 3661, 3685, and 3739 cm^{-1} in the deposition spectra, that we attribute to $Fe:H_2O$ and $Fe_2:H_2O$ by comparison with their calculated IR spectra (see Figure 2, left-hand panel inset,

and Table 1). In our experiments with D_2O, the ν_3 at 3661 and 3739 cm^{-1} are shifted to 2675 and 2716 cm^{-1}, respectively (see Table 3). In the UV-visible, we observe known bands of Fe and Fe_2 in the pure argon matrix.[56,57] As the concentration of water in the matrix increases, we observe the presence of other bands which we attribute to Fe:H_2O, as highlighted in Figure 2, right-hand panel inset. These bands are attributed based upon our calculation of the electronic spectrum (see Table 2 and the discussion below) as no literature data was available. It should be noted that we did not calculate the electronic spectrum of Fe_2:H_2O (which gives rise to the observed bands at 414 and 468 nm) because of the number of active electrons and orbitals (16, 24) that must be taken into account, leading to an inaccessible active space for the CASSCF/CASPT2 method. The intensity of the experimental IR and UV-visible absorption bands increases with H_2O concentration in the matrices, indicating the presence of a larger number of adducts upon deposition. Annealing of the matrices had only a minimal impact on the water aggregates, largely some accelerated conversion between the ortho and para forms of H_2O, and no apparent effect on the concentration of Fe:H_2O and Fe_2:H_2O adducts.

The BPW91/cc-pVTZ optimised geometries of the various iron:water adducts that were initially considered as being potentially formed in the experiments, and for which the harmonic IR spectra were computed, are presented in Figure 3 along with the natural electronic population on the Fe atom within the complexes. All computed geometries and harmonic spectra for hydrogenated and deuterated complexes are reported in Table S3 in the SI. The energetics of the reactions forming adducts from iron atoms/dimers and water molecules are reported in Table 4. We identified a ^{5}A" state to be the most stable one for the Fe:H_2O complex. The geometrical parameters are slightly different from those determined – using the B3LYP functional – by Zhang *et al.*,[12] who found a ^{5}A' ground state. Concerning energetics, we found a complexation energy of -39 kJ mol^{-1} at the DFT level, which diminishes to -16 kJ mol^{-1} at the CCSD(T)//DFT level. The former value is in agreement with that computed by Karlicky and Otyepka at the same level of theory (see Table 5 in Ref.[21]). These authors also found a decrease of the complexation energy using a CCSD(T) hamiltonian, amounting to -7.5 kJ mol^{-1} using a large basis set (CCSD(T)/cc-pwCVnz-DK). It is interesting to note that Zhang *et al.* calculated an exothermicity of -56 kJ mol^{-1} with the B3LYP functional[12] whereas Karlicky and Otyepka determined a value of -38 kJ mol^{-1} at the B3LYP level of theory using a cc-pVTZ basis set (Table 5 in Ref.[21]). Regarding the formation of the complex, as there is no spin change between reactants and product, no barrier is expected to be present.

As can be seen in Table 1, the wavenumber associated with the ν_{aOH} mode for the ^{5}A" Fe:H_2O complex is particularly low in energy (even slightly lower, by 11 cm^{-1}, than the experimental value) and much lower than B3LYP values mentioned in the literature. This may be due to a questionable description of long-range interactions in the BPW91 potential. Indeed, harmonic frequencies of water were determined to be 1613, 3705 and 3807 cm^{-1} at the BPW91/cc-pVTZ level, while experimental gas phase values are 1594, 3657 and 3756 cm^{-1}.[62] We may note that the agreement between both is obtained with scaling factors of 0.988, 0.987 and 0.986 respectively. Upon coordination to the Fe atom, the ν_{sOH} and ν_{aOH} values appear red-shifted by 157 cm^{-1} and 160 cm^{-1} at the BPW91/cc-pVTZ level, respectively, which is surely overestimated. This means that, upon interaction with Fe, the OH bond are overly weakened, and this has a larger effect on stretching than bending modes. Adding empirical dispersion corrections leads to an increase by 11 cm^{-1} of the ν_{aOH} mode, 7 cm^{-1} of the ν_{sOH} mode, and 2 cm^{-1} of the δ_{OH_2} mode. The inclusion of dispersion interactions thus improves the calculated positions of the IR bands, especially those of the stretching OH bands, with respect to experimental data. It should be noted that the geometry changes induced by dispersion are small, the Fe-O bond being increased by 0.01 Å and the Fe-OH angle by 2° (from 104° to 106°). Dispersion effects

stabilise the complex by 5 kJ mol^{-1} at the DFT level, but single point CCSD(T) calculations for the DFT-D geometry lead to a destabilisation of 3 kJ mol^{-1} with respect to the initial CCSD(T)/DFT value (see the first line of Table 4). The inclusion of dispersion interactions thus increases the discrepancies between DFT and CCSD(T)//DFT values in terms of the energetics.

Based upon MS-CASPT2 calculations, the 15 first quintet electronic states of the Fe:H_2O adduct can be identified as the slightly mixed $3d^64s^2$ and $3d^74s$ configurations of the iron and beyond these, the presence of the water molecule gives rise to strong mixing between the $3d^64s4p$ and the $3d^74p$ configurations. The spin-orbit coupling of the 70 electronic states leads to 350 spin-orbit states. Spin-orbit states as well as energies and oscillator strengths, with relative oscillator strengths (compared to the maximal 0.076 value) higher than 0.013, are given in Table 2. The oscillator strengths are overall larger than those of the atomic iron and more spin-orbit states absorb. The most intense band, corresponding to a $3d^64s4p$ electronic configuration, is found 20 nm lower than for the iron atom (280.6 nm instead of 300.7 nm).

Returning to the DFT geometries, for complexes of Fe with two water molecules, we considered two types of isomers: one with a water dimer interacting with Fe (see Figure 3, lower left), hereafter designated $Fe(H_2O)_2$, and a second with two individual water molecules coordinated to the Fe atom via their oxygen atoms (see Figure 3, lower middle), hereafter designated $(H_2O)Fe(H_2O)$. We considered only a quintet spin state for $Fe(H_2O)_2$, analogous to $Fe(H_2O)$. In the optimised geometry, one water molecule is coordinated to the Fe atom *via* its oxygen and the second molecule interacts with Fe through the H atom not involved in the hydrogen bond with the first water molecule. Such a structure resembles the "filament" isomer found for $[Fe(H_2O)_2]^+$ by Garza-Galindo and co-workers,[63] although in this cationic species the second water molecule does not interact at all with Fe^+. Regarding energetics, the formation of $Fe(H_2O)_2$ is thermodynamically favourable from one Fe atom and two water molecules, as it would be exothermic by -52 kJ mol^{-1} at the CCSD(T)//DFT level of theory. As in the case of $Fe(H_2O)$, no spin change occurs during the complexation and therefore no energetic barrier is expected. For the $(H_2O)Fe(H_2O)$ isomer, we found two low energy spin states: a quintet and a triplet. The latter was found to be the most stable at the DFT level, while the former was lower in energy at the CCSD(T)//DFT level (see Table 4). In the final optimised geometry of the triplet spin state, the Fe atom is aligned with the O atoms, as found for $(H_2O)Fe(H_2O)^+$,[63] whereas the O-Fe-O angle in the quintet is 124°. Contrary to the results for the cation, the Fe, O and two H atoms for a given water ligand are not in the same plane. This was expected, as such a difference has already been observed between the $Fe(H_2O)$ and $Fe(H_2O)^+$ complexes. In terms of energetics, DFT calculations indicate that the formation of the two isomers is exothermic, although single point CCSD(T) calculations indicate an endothermic process for the triplet (+27 kJ mol^{-1}, and a slightly exothermic process for the quintet (-3.5 kJ mol^{-1}). We note here that the two isomers present different stretching OH features: the combination of symmetric OH stretching modes are found at3502/3507 cm^{-1} for the quintet and 3403/3417 cm^{-1} for the triplet, while the combination of antisymmetric ones are found at 3606/3607 cm^{-1} for the quintet and at 3476/3493 cm^{-1} for the triplet. None of these positions are in agreement with experimental data. Taking into account dispersion effects for such complexes induces very small changes in the harmonic IR mode positions (maximum shift of +11 cm^{-1} observed for the ν_{aOH} of $(H_2O)Fe(H_2O)$ ^{5}A). This is associated with tiny geometrical changes (see Table S3 in the SI) and stabilisation (resp. destabilisation) at the DFT (resp. CCSD(T)) levels of theory. We only observe that the $Fe(H_2O)_2$ complex is more stabilised than the others when dispersion is included (see Table 4), which is probably due to the presence of the weakly bound water dimer.

We also considered the complex formed between the Fe dimer and one water molecule. For Fe_2:H_2O, we found a ^{7}A' ground state at the DFT level, with Fe-Fe-O slightly deriving from linearity (see Figure 3, top right). Both spin state and geometry are similar to those found by Zeinalipour-Yazdi and van Santen,[1] with a maximum difference in the geometrical parameters of 0.02 Å (in the Fe_2-O bond length). We found a Fe_2-H_2O interaction energy of -47 kJ mol^{-1} at the DFT level of theory while those authors found -10 kcal mol^{-1} (about -42 kJ mol^{-1}). At the CCSD(T)//DFT level, the formation of this complex in its ^{7}A' state becomes endothermic (+14 kJ mol^{-1}). In fact, in contrast to the results of Zeinalipour-Yazdi and van Santen,[1] we found a nonuplet spin state for Fe_2:H_2O with a different geometry from that of the ^{7}A' state, and lying +59 kJ mol^{-1} above it at the DFT level (see Figure 3 and Table 4). This nonuplet complex is, however, found to be stable at the CCSD(T)//DFT level, leading to a Fe_2-H_2O complexation energy of -26 kJ mol^{-1} (see Table 4). This was expected, as the ground state of Fe_2 was found to be $^7\Delta_u$ at the DFT level (ΔE = 55 kJ mol^{-1}) and $^9\Sigma_g^-$ at the CCSD(T)//DFT level (ΔE = 95 kJ mol^{-1}). This type of calculation illustrates the limitation of DFT treatment for complexes involving transition metal clusters. The formation of Fe_2:H_2O from the reactants Fe_2 + H_2O should be energetically favourable, and no energetic barrier is expected to be present (no spin change). We may notice that, as the differences in the vibrational frequencies of the ^{7}A' and ^{9}A isomers are of the same order of magnitude as the uncertainties in the DFT mode positions, it is not possible to determine which isomer is formed in the experiment. Taking into account dispersion effects leads to the same conclusions as for the Fe:H_2O complexes: it leads to very small changes in harmonic mode positions (less than 5 cm^{-1}) and geometries, while the discrepancies between DFT and CCSD(T)/DFT energetics are increased. Overall, taking into account dispersion interactions does not modify the conclusions of the comparison between experiment and theory. For the current study, it is likely that the fact that calculations are performed on gas phase molecules and complexes, and thus the matrix effects are not taken into account, is a larger source of discrepancy than the consideration of dispersion interactions.

Photoproducts of Fe adducts with H_2O

The experimental IR and UV-visible spectra recorded after UV irradiation of matrices containing iron:water adducts are presented in Figures 4 and 5. The adducts Fe:H_2O and Fe_2:H_2O are removed from the argon matrices, as evidenced by the disappearance of absorption bands attributed to these species. The loss of the bands at 3661, 3685, and 3739 cm^{-1} in the ν_3/ν_1 OH stretching region of the mid-IR confirms their attribution to Fe adducts. Similarly, in the UV-visible spectra, the bands at 270, 281, 320, 324, 331, 342, 356, 372, 387, 430, and 451 nm are confirmed to be due to Fe adducts. The assignments of the IR bands, based on comparison with DFT calculations, are reported in Table 1. Similar data for their deuterated counterparts are reported in Table 3.

The loss of Fe adducts in the matrices coincides with the appearance of new absorption bands due to the formation of insertion photoproducts. In the ν_2 OH bending mode region (Figure 4, left-hand panel), new absorption features are observed at 1733 and 1712 cm^{-1}. As in previous studies,[11,12] these are attributed to the insertion products HFeOH and HFeOFeH, respectively. These species also give rise to bands at 682 and 458 cm^{-1} and at 914 cm^{-1}, respectively (see Figure 4 and Table 1). In this work, we have identified bands of photoproducts in the ν_3/ν_1 OH stretching region for the first time based on our experimental spectra and quantum chemistry calculations. An absorption feature at 3742 cm^{-1} is attributed to HFeOH.

In addition to insertion photoproducts, two further species are identified in the experimental spectra. Firstly, $Fe(OH)_2$ gives rise to absorption features at 737, 631, and 513 cm^{-1}, identified in previous studies,[11,12] and at 3728 cm^{-1}, identified here for the first time based upon our DFT calculations. Secondly,

the absorption feature at 873 cm^{-1} is attributed to FeO,[53,54] observed in the study of Zhang *et al.*[12] but not that of Kauffman *et al.*[11] In the same spectral region, we observe a few minor peaks which are low intensity, but which increase with the concentration of H_2O in the matrix. These are all in the region where we expect to see absorptions due to O-Fe-O (for example Zhang *et al.*[12] propose HFeOFeOH as the attribution for the band at 695 cm^{-1}), so we tentatively assign them to multiple insertion species without providing a precise attribution.

The BPW91/cc-pVTZ optimised geometries of the theoretically-treated photoproducts are presented in Figure 6, and the thermodynamics of their formation from the Fe atom/dimer and water molecule(s) can be found in Table 4. All computed geometries and harmonic spectra for hydrogenated and deuterated complexes are reported in Table S4 in the SI. The energetics of the reactions forming adducts from iron atoms/dimers and water molecules are reported in Table 4. The ground state of the complex resulting form the insertion of the Fe atom into one O-H bond of the water molecule, HFeOH, was determined to be a ^{5}A" state, lying 120 kJ mol^{-1} below the Fe:H_2O complex at the DFT level of theory. We note that Gutsev *et al.* determined an energy difference of 104 kJ mol^{-1} between HFeOH – for which they found two degenerate ^{5}A' and ^{5}A" complexes as the most stable – and Fe:H_2O (^{5}A'), using the same functional as us (BPW91) but a different basis set (6-311+G**).[20] We concluded that the formation of HFeOH from Fe + H_2O was exothermic by 159 kJ mol^{-1} at the DFT level, and by 129 kJ mol^{-1} at the CCSD(T)//DFT level. These values are consistent with those obtained by Karlicky and Otyepka.[21] These authors also computed the reaction path leading to HFeOH from Fe + H_2O and showed that the insertion of Fe into the O-H water bond cost 99 kJ mol^{-1} (Figure 3 in Ref.[21]). They also determined the reaction path that leads from HFeOH to the formation of FeO and H_2, and showed that it cost 151 kJ mol^{-1} with respect to Fe + H_2O. In agreement with this prior study,[21] we found the relative energy of FeO + H_2 with respect to Fe + H_2O to be significantly underestimated at the BPW91/cc-pVTZ level of theory (-29 kJ mol^{-1} vs +113 kJ mol^{-1} at the CCSD(T)//DFT level, see Table 4).

The insertion of Fe_2 into a O-H bond may lead to the formation of HFe_2OH. We found that the lowest energy spin state for this complex at the BPW91/cc-pVTZ level corresponded to a septuplet state. In the optimised geometry, the lone H atom interacts with the two Fe atoms, whereas the OH is coordinated to only one Fe atom (see Figure 6, centre left image). Interestingly, this spin state/geometry is similar to that found by Zeinalipour-Yazdi and van Santen (B3LYP calculations)[1] with, however, small discrepancies in the bond lengths, up to a maximum of 0.3 Å in the Fe-Fe bond, with distances in B3LYP being larger than those in BPW91. In the most stable geometry obtained for this type of isomer by Gutsev *et al.*,[20] both H atoms and the O atom interact with the two Fe atoms. We optimised the same isomer, finding it to lie 41 kJ mol^{-1} higher in energy than our most stable one. We also optimised a nonuplet spin state starting from the ^{7}A ground state geometry. The geometry was slightly distorted (see Figure 6, lower left image), and the ^{9}A complex was found to lie 51 kJ mol^{-1} above the ^{7}A one at the DFT level. However, when performing CCSD(T)//DFT calculations, the ^{9}A complex was found to be the ground state (ΔE=-32 kJ mol^{-1} with respect to the septuplet). The formation of both complexes was found to be exothermic. Here, we underline that Zeinalipour-Yazdi and van Santen showed that the formation of the HFe_2OH complex from Fe_2:H_2O in their septuplet spin states would require about 24 kJ mol^{-1} at the B3LYP level (see Figure 5b of Ref.[1]), which is, interestingly, much lower than the activation energy calculated for one Fe atom. However, one has to be careful about these results because, as discussed above, DFT methods are likely to highly underestimate energetic barriers.

Finally, we optimised the geometries of other complexes whose formation paths from Fe atoms and water molecules are not trivial, namely the complexes HOFeOH and HFeOFeH,

also suggested to be formed in the experiment of Zhang *et al.*[12] We found quintet and nonuplet spin states for the ground states of these complexes, respectively, in agreement with the calculations of Zhang *et al.*[12] The final optimised geometry of HOFeOH is quite similar to that obtained by Zhang *et al.*, except that we find a Fe-O-H angle smaller by 10°. For HFeOFeH, we found a H-Fe-O angle of 177° while Zhang *et al.* had proposed a strictly linear structure. Both HOFeOH and HFeOFeH complexes were found to be very stable with respect to the initial reactants, -225 and -288 kJ mol^{-1} at the CCSD(T)//DFT level, respectively. We compared the energetics for the formation of HOFeOH (Fe + $2H_2O \rightarrow$ HOFeOH+H_2) and HFeOFeH (Fe + HFeOH $\rightarrow$ HFeOFeH) computed in the present work with values obtained by Zhang *et al.*[12] using the B3LYP functional. For HOFeOH, we obtained -266 (resp. -225) kJ mol^{-1} at the DFT (resp. CCSD(T)//DFT) level, whereas Zhang *et al.* obtained a value of -262 kJ mol^{-1}. For HFeOFeH, we obtained -174 (resp. -159) kJ mol^{-1} at the DFT (resp. CCSD(T)//DFT) level, whereas Zhang *et al.* obtained a value of -192 kJ mol^{-1}. Therefore, while the calculated energetics for the formation of $Fe(OH)_2$ are very similar in both studies, we obtained smaller values for the formation of HFeOFeH.

There was no observation of photoproducts in the UV-visible spectrum, although the loss of Fe_{1-2}:H_2O adducts from the matrix was confirmed by the disappearance of their absorption bands (as can be verified in Figure 5, right-hand panel). The ground state obtained at the MS-CASPT2 level for the HFeOH complex is ^{5}A" $H^-Fe^{2+}(3d^6)O^-H$. It appears that the first four quintet excited states correspond to metal centered transitions $d_{z^2} \rightarrow d_{xz}$ (41 cm^{-1} or 242359 nm); $d_{z^2} \rightarrow d_{x^2-y^2}$ (4119 cm^{-1} or 2428 nm); $d_{z^2} \rightarrow d_{yz}$ (4999 cm^{-1} or 2000 nm); $d_{z^2} \rightarrow d_{xy}$ (6326 cm^{-1} or 1581 nm). The following states are of different natures: excitation from the terminal hydrogen to the iron 3d or 4p orbitals, excitation centered on the iron, from a 3d orbital to the 4p orbital, and finally excitation from the oxygen lone pair to the 3d orbitals of the iron atom. However, the oscillator strengths are very weak for all the states until 245 nm (see Table S5 in the SI), which could explain why no absorption bands in the experimentally accessible UV-visible region were observed for this species. States corresponding to an excitation from the oxygen lone pair to the 3d orbitals of the iron atom and local excitation on the iron atom (3d to 4p) are found lower than 245 nm with a significant oscillator strength. In Figure 7, we present the calculated electronic spectra of Fe, Fe:H_2O and HFeOH. It should be noted that the calculated band positions present a very good agreement with the experimental data, especially given the fact that the experimental spectra were measured in cryogenic matrices and that the calculations did not take into account anharmonicity. It should also be noted that electronic spectra were not calculated for the other confirmed photoproducts (HFeOFeH, $Fe(OH)_2$, FeO), as this would represent an extensive study in itself.

Experiments and calculations using deuterated water confirm the attributions made here for Fe:H_2O, Fe_2H_2O, HFeOH and FeO. It should be noted that our calculations were made without taking account of the anharmonicity and the effect of the argon matrix on the frequencies. However, a very good agreement was obtained, particularly for D_2O and deuterated Fe-containing compounds, for which anharmonicity effects are reduced (see Table 3 for details of attributions, or Tables S3 and S4 in the SI for a complete list of calculated deuterated species).

Conclusions

Using a combined experimental and theoretical approach, we have determined, for the first time, the UV-visible and 3800 – 3600 cm^{-1} mid-IR spectra of Fe_x:H_2O_y adducts and their photoproducts (including the insertion species HFeOH, HFeOFeH and the molecules $Fe(OH)_2$ and FeO). By applying the results of DFT calculations to our experimental mid-IR spectra, building upon our knowledge of the IR spectroscopy of water clusters,[58] we were able to attribute bands to OH stretches of Fe adducts and insertion products. Using the SO-CASPT2

or SO-MS-CASPT2 method and our previous work on iron complexes,[51] we were able to model the Fe, Fe:H_2O and HFeOH UV-visible spectra. Despite the lack of matrix effects or anharmonicity (for IR spectra) in the theoretical description, both computed mid-IR and UV-visible spectra well reproduced the experimental spectra. In order to verify the higher energy transitions, especially for HFeOH, we intend to extend these experiments to lower wavelengths by changing the experimental setup.

The experiments presented here confirm that atomic Fe in its neutral state is highly reactive with water. We observed the production of photoproducts, even for the lowest concentrations of H_2O, despite the fact that irradiation of matrices was only carried out for three minutes at an average power of $\sim$ 150 mW. This suggests that the reaction could potentially be very important in dense astrophysical regions irradiated by UV. The identification of spectral bands in the mid-IR and UV-visible regions may also help with the identification of iron-bearing species in such interstellar environments.

Acknowledgement This work has been funded by the Agence Nationale de la Recherche (ANR) project "PARCS" ANR-13-BS08-0005, with support from the French research network EMIE (Edifices Moléculaires Isolés et Environnés, GDR 3533), and the French Programme National "Physique et Chimie du Milieu Interstellaire" (PCMI) of CNRS/INSU with INC/INP co-funded by CEA and CNES. We acknowledge the help of Fode Fall and the computing facility CALMIP at the Paul Sabatier University in Toulouse. NB thanks H. Bolvin for helpful discussions.

Supporting Information Available: The validation of the CASPT2 parameters is presented in the SI, accompanied by Table S1. Experimental and SO-CASPT2 energy levels of Neutral Iron atom are given in Table S2. The complete list of calculated frequencies for hydrogenated and deuterated species (without and with dispersion) are presented in Tables S3 and S4. The calculated absorption energies of HFeOH are presented in Table S5. This material is available free of charge via the Internet at `http://pubs.acs.org/`.

References

(1) Zeinalipour-Yazdi, C. D.; van Santen, R. A. Kinetic Rates and Linear Free Energy Relationships for Water Dissociation on Transition and Noble Metal Dimers. *J. Phys. Chem. A* **2009**, *113*, 6971–6978.

(2) Plane, J. M. C.; Feng, W.; Dawkins, E. C. M. The Mesosphere and Metals: Chemistry and Changes. *Chem. Rev.* **2015**, *115*, 4497–4541.

(3) McDonald, I.; Sloan, G. C.; Zijlstra, A. A.; Matsunaga, N.; Matsuura, M.; Kraemer, K. E.; Bernard-Salas, J.; Markwick, A. J. Rusty Old Stars: A Source of the Missing Interstellar Iron? *Astrophys. J. Lett.*, **2010**, *717*, L92.

(4) Magnera, T. F.; David, D. E.; Michl, J. Gas-phase Water and Hydroxyl Binding-energies for Monopositive 1st Row Transition-metal Ions *J. Am. Chem. Soc.*, **1989**, *111*, 4100-4101.

(5) Marinelli, P. J.; Squires, R. R. Sequential Solvation of Atomic Transition-metal Ions – The 2nd Solvent Molecule Can Bind More Strongly Than the 1st *J. Am. Chem. Soc.*, **1989**, *111*, 4101-4103.

(6) Dukan, L.; del Fabbro, L.; Pradel, P.; Bublemontier, O.; Mestdagha, J. M.; Visticot, J. P. Photofragmentation of Hydrated Iron Ions $Fe(H_2O)_n^+$ (n = 1–9) at 532, 355 and 266 nm *Eur. Phys. J. D*, **1998**, *3*, 257–265.

(7) Walters, R. S.; Duncan M. A. Infrared Spectroscopy of Solvation and Isomers in $Fe^+(H_2O)_{1,2}Ar_m$ Complexes *Aust. J. Chem.*, **2004**, *57*, 1145–1148.

(8) van der Linde, C.; Beyer, M. K. Reactions of $M^+(H_2O)_n$, n < 40, M = V, Cr, Mn, Fe, Co, Ni, Cu, and Zn, with D_2O Reveal Water Activation in $Mn^+(H_2O)_n$ *J. Phys. Chem. A*, **2012**, *116*, 10676–10682.

(9) Ohashi, K.; Sasaki, J.; Yamamoto, G.; Judai, K.; Nishi, N.; Sekiya, H. Temperature Effects on Prevalent Structures of Hydrated Fe^+ Complexes: Infrared Spectroscopy and DFT Calculations of $Fe^+(H_2O)_n$ (n = 3–8) *J. Chem. Phys.*, **2014**, *141*, 214307.

(10) Kiawi, D. M.; Chernyy, V.; Oomens, J.; Buma, W. J.; Jamshidi, Z.; Visscher, L.; Waters, L. B. F. M.; Bakker, J. M. Water Dissociation upon Adsorption onto Free Iron Clusters Is Size Dependent *J. Phys. Chem. Lett.*, **2016**, *7*, 2381–2387.

(11) Kauffman, J. W.; Hauge, R. H.; Margrave, J. L. Studies of Reactions of Atomic and Diatomic Cr, Mn, Fe, Co, Ni, Cu, and Zn with Molecular Water at 15 K *J. Phys. Chem.*, **1985**, *89*, 3541–3547.

(12) Zhang, L.; Zhou, M.; Shao, L.; Wang, W.; Fan, K.; Qin, Q. Reactions of Fe with H_2O and FeO with H_2. A Combined Matrix Isolation FTIR and Theoretical Study *J. Phys. Chem. A*, **2001**, *105*, 6998–7003.

(13) Weiller, B. H.; Bechthold, P. S.; Parks, E. K.; Pobo, L. G.; Riley, S. J. The Reactions of Iron Clusters with Water *J. Chem. Phys.*, **1989**, *91*, 4714.

(14) Liu, S.; Tian, X.; Wang, T.; Wen, X.; Li, Y.-W.; Wang, J.; Jiao, H. High Coverage Water Aggregation and Dissociation on Fe(100): A Computational Analysis *J. Phys. Chem. C*, **2014**, *118*, 26139–26154.

(15) Liu, S.; Tian, X.; Wang, T.; Wen, X.; Li, Y.-W.; Wang, J.; Jiao, H. Coverage Dependent Water Dissociative Adsorption on the Clean and O-Precovered Fe(111) Surfaces *J. Phys. Chem. C*, **2015**, *119*, 11714–11724.

(16) Liu, S.; Tian, X.; Wang, T.; Wen, X.; Li, Y.-W.; Wang, J.; Jiao, H. Coverage Dependent Water Dissociative Adsorption on Fe(110) from DFT Computation *Phys. Chem. Chem. Phys.*, **2015**, *17*, 8811–8821.

(17) Liu, S.; Li, Y.-W.; Wang, J.; Jiao, H. Reaction of CO, H_2O, H_2 and CO_2 on the Clean as Well as O, OH and H Precovered Fe(100) and Fe(111) Surfaces *Catal. Sci. & Technol.*, **2017**, *7*, 427–440.

(18) Becke, A. D. Density-functional Exchange-energy Approximation with Correct Asymptotic Behavior *Phys. Rev. A*, **1988**, *38*, 3098–3100.

(19) Perdew, J. P.; Wang, Y. Accurate and Simple Analytic Representation of the Electron-gas Correlation Energy *Phys. Rev. B*, **1992**, *23*, 13244–13249.

(20) Gutsev, G. L.; Mochena, M. D.; Bauschlicher, C. W. Jr. Interaction of Water with Small Fe_n Clusters *Chem. Phys.*, **2005**, *314*, 291–298.

(21) Karlicky, F.; Otyepka, M. First Step in the Reaction of Zerovalent Iron with Water *J. Chem. Theory Comput.*, **2011**, *7*, 2876–2885.

(22) Lanza, M.; Simon, A.; Ben Amor, N. Electronic Spectroscopy of $[FePAH]^{(+)}$ Complexes in the Region of the Diffuse Interstellar Bands: Multireference Wave Function Studies on $[FeC_6H_6]^{(+)}$ *J. Phys. Chem. A*, **2015**, *119*, 6123–6130.

(23) Tremblay, B.; Gutsev, G.; Manceron, L.; Andrews, L. Vibrational Spectrum and Structure of the Fe_2CO molecule. An Infrared Matrix Isolation and Density Functional Theory Study *J. Phys. Chem. A*, **2002**, *106*, 10525–10531.

(24) Tremblay, B.; Manceron, L.; Gutsev, G. L.; Andrews, L.; Partridge, H. Experimental and Theoretical Infrared Spectra of Co_2CO *J. Chem. Phys.*, **2002**, *117*, 8479–8485.

(25) Grimme, S. ; Semiempirical GGA-Type Density Functional Constructed with a Long-Range Dispersion Correction *J. Comput. Chem.*, **2006**, *27*, 1787–1799.

(26) Meza B.; Miranda P. ;Castro, M.; Structural and Electronic Properties of Hydrated V_nH_2O and $V_n{}^+H_2O$, n$\leq$ 13, Systems *J. Phys. Chem. C*, **2017**, *121*, 4635–4649.

(27) Frisch, M. J.; Trucks, G. W.; Schlegel, H. B.; Scuseria, G. E.; Robb, M. A.; Cheeseman, J. R.; Scalmani, G.; Barone, V.; Mennucci, B.; Petersson, G. A. *et al. Gaussian 09*, Revision A.1; Gaussian, Inc.: Wallingford, CT, **2009**.

(28) Aquilante, F.; De Vico, L.; Ferré, N.; Ghigo, G.; Malmqvist, P.-Å.; Neogrady, P.; Pedersen, T. B.; Pitonak, M.; Reiher, M.; Roos, B. O. *et al.* Software News and Update MOLCAS 7: The Next Generation *J. Comput. Chem.*, **2010**, *31*, 224–247.

(29) Karlström, G.; Lindh, R.; Malmqvist, P.-Å.; Roos, B. O.; Ryde, U.; Veryazov, V.; Widmark, P. O.; Cossi, M.; Schimmelpfennig, B.; Neogrady, P. *et al.* MOLCAS: A Program Package for Computational Chemistry *Comput. Mater. Sci.*, **2003**, *28*, 222–239.

(30) Veryazov, V.; Widmark, P.-O.; Serrano-Andrés, L.; Lindh, R.; Roos, B. O. MOLCAS as a Development Platform for Quantum Chemistry Software *Int. J. Quantum Chem.*, **2004**, *100*, 626–635.

(31) Roos, B. O.; Lindh, R.; Malmqvist, P.-Å.; Veryazov, V.; Widmark, P.-O. Main Group Atoms and Dimers Studied with a New Relativistic ANO Basis Set *J. Phys. Chem. A*, **2004**, *108*, 2851–2858.

(32) Roos, B. O.; Lindh, R.; Malmqvist, P.-Å.; Veryazov, V.; Widmark, P.-O. New Relativistic ANO Basis Sets for Transition Metal Atoms *J. Phys. Chem. A*, **2005**, *109*, 6575–6579.

(33) Douglas, M.; Kroll, N. M. Quantum Electrodynamical Corrections to the Fine Structure of Helium *Ann. Phys.*, **1974**, *82*, 89–155.

(34) Jansen, G.; Hess, B. A. Revision of the Douglas-Kroll Transformation *Phys. Rev. A*, **1989**, *39*, 6016–6017.

(35) Roos, B. O.; Taylor, P. R.; Sigbahn, P. E. A Complete Active Space SCF Method (CASSCF) Using a Density Matrix Formulated Super-CI Approach *Chem. Phys.*, **1980**, *48*, 157–173.

(36) Andersson, K.; Malmqvist, P.-Å.; Roos, B. O.; Sadlej, A. J.; Wolinski, K. Second-Order Perturbation Theory with a CASSCF Reference Function *J. Phys. Chem.*, **1990**, *94*, 5483–5488.

(37) Finley, J.; Malmqvist, P.-Å.; Roos, B. O. & Serrano-Andrés, L. The multi-state CASPT2 method *Chem. Phys. Lett.*, **1998**, *288*, 299–306.

(38) Aquilante, F.; Pedersen, T. B.; Lindh, R. Low-Cost Evaluation of the Exchange Fock Matrix from Cholesky and Density Fitting Representations of the Electron Repulsion Integrals *J. Chem. Phys.*, **2007**, *126*, 194106.

(39) Aquilante, F.; Malmqvist, P.-Å.; Pedersen, T. B.; Ghosh, A.; Roos, B. O. Decomposition-Based Multiconfiguration Second-Order Perturbation Theory (CD-CASPT2): Application to the Spin-State Energetics of Co^{III} (Diiminato)(NPh) *J. Chem. Theory Comput.*, **2008**, *4*, 694–702.

(40) Malmqvist, P.-Å.; Roos, B. O.; Schimmelpfennig, B. The Restricted Active Space (RAS) State Interaction Approach with Spin–orbit Coupling *Chem. Phys. Lett.*, **2002**, *357*, 230–240.

(41) Autillo, M.; Guerin, L.; Guillaumont, D.; Moisy, P.; Bolvin, H.; Berthon, C. Paramagnetism of Aqueous Actinide Cations. Part II: Theoretical Aspects and New Measurements on An(IV) *Inorg. Chem.*, **2016**, *23*, 121459–12157

(42) Ghigo, G.; Roos, B. O.; Malmqvist, P.-Å. A Modified Definition of the Zeroth-Order Hamiltonian in Multiconfigurational Perturbation Theory (CASPT2) *Chem. Phys. Lett.*, **2004**, *396*, 142–149.

(43) Kerridge, A. A RASSCF Study of Free Base, Magnesium and Zinc Porphyrins: Accuracy versus Efficiency *Phys. Chem. Chem. Phys.*, **2013**, *15*, 2197–2209.

(44) Vela, S.; Fumanal, M.; Ribas-Ariño, J.; Robert, V. On the Zeroth-Order Hamiltonian for CASPT2 Calculations of Spin Crossover Compounds *J. Comput. Chem.*, **2016**, *37*, 947–953.

(45) Kepenekian, M.; Robert, V.; Le Guennic, B. What Zeroth-Order Hamiltonian for CASPT2 Adiabatic Energetics of $Fe(II)N_6$ Architectures? *J. Chem. Phys.*, **2009**, *131*, 114702.

(46) Radoń, M.; Rejmak, P.; Fitta, M.; Bałanda, M.; Szklarzewicz, J. How Can $[Mo^{IV}(CN)_6]^{2-}$, an Apparently Octahedral $(d)^2$ Complex, Be Diamagnetic? Insights from Quantum Chemical Calculations and Magnetic Susceptibility Measurements *Phys. Chem. Chem. Phys.*, **2015**, *17*, 14890–14902.

(47) Ruipérez, F.; Aquilante, F.; Ugalde, J. M.; Infante, I. Complete vs Restricted Active Space Perturbation Theory Calculation of the Cr_2 Potential Energy Surface *J. Chem. Theory Comput.*, **2011**, *7*, 1640–1646.

(48) Vancoillie, S.; Malmqvist, P. Å.; Veryazov, V. Potential Energy Surface of the Chromium Dimer Re-Re-Revisited with Multiconfigurational Perturbation Theory *J. Chem. Theory Comput.*, **2016**, *12*, 1647–1655

(49) Zobel, J. P.; Nogueira, J. J.; Gonzalez, L. The IPEA Dilemma in CASPT2 *Chem. Sci.*, **2017**, *8*, 1482–1499.

(50) Wiebeler, C.; Borin, V.; Sanchez de Araújo, A. V.; Schapiro, I.; Borin, A. C. Excitation Energies of Canonical Nucleobases Computed by Multiconfigurational Perturbation Theories *Photochem. Photobiol.*, **2017**, *93*, 888–902.

(51) Ben Amor, N.; Soupart, A.; Heitz, M.-C. Methodological CASPT2 Study of the Valence Excited States of an Iron-Porphyrin Complex. *J. Mol. Model.*, **2017**, *23* (2).

(52) Mebel, A. M.; Hwang, D. Y. Theoretical Study of the Reaction Mechanism of Fe Atoms with H_2O, H_2S, O_2 and H^+ *J. Phys. Chem. A*, **2001**, *105*, 7460–7467.

(53) Green, D. W.; Reedy, G. T.; Kay, A. G. Matrix-Isolated FeO, NiO, and CoO Ground-State Vibrational Frequencies *J. Mol. Spec.*, **1979**, *78*, 257–266.

(54) Chang, S.; Blyholder, G.; Fernandez, J. Iron-Oxygen Interactions in an Argon Matrix *Inorg. Chem.*, **1981**, *20*, 2813–2817.

(55) Nave, G.; Johansson, S.; Learner, R. C. M.; Thorne, A. P.; Brault, J. W. A New Multiplet Table for Fe-I *Astrophys. J. Suppl. Ser.*, **1994**, *94*, 221–459.

(56) Mann, D. M.; Broida, H. P. Ultraviolet Absorption Spectra of Transition Metal Atoms in Rare Gas Matrices *J. Chem. Phys.*, **1971**, *55*, 84–94.

(57) de Vore, T. C.; Ewing, A.; Franzen, H. F.; Calder, V. The Visible Absorption Spectra of Mn_2, Fe_2, and Ni_2 in Argon Matrices *Chem. Phys. Lett.*, **1975**, *35*, 78–81.

(58) Simon, A.; Noble, J. A.; Rouaut, G.; Moudens, A.; Aupetit, C.; Iftner, C.; Mascetti, J. Formation of Coronene:water Complexes: FTIR Study in Argon Matrices and Theoretical Characterisation *Phys. Chem. Chem. Phys.*, **2017**, *19*, 8516–8529.

(59) Demovič, L.; Kellö, V.; Urban, M. Relativistic Effects in Low-Lying Electronic States of Iron *Theor. Chem. Acc.* **2011**, *129*, 561–566.

(60) Bentwood, R. M.; Barnes, A. J.; Orville-Thomas, W. J. Studies of Intermolecular Interactions by Matrix-Isolation Vibrational Spectroscopy – Self-Association of Water *J. Mol. Struct.*, **1980**, *84*, 391–404.

(61) Coussan, S.; Roubin, P.; Perchard, J. P. Infrared induced isomerizations of water polymers trapped in nitrogen matrix *Chem Phys*, **2006**, *324*, 527–540.

(62) Benedict, W. S.; Gailar, N.; Plyler, E. K. ; RotationVibration Spectra of Deuterated Water Vapor *J. Chem. Phys.*, **1956**, *24*, 1139–1165.

(63) Garza-Galindo, R.; Castro, M.; Duncan, M. A. Theoretical Study of Nascent Hydration in the $Fe^+(H_2O)_n$ System *J. Phys. Chem. A*, **2012**, *116*, 1906–1913.

Table 1: Attribution of IR spectral bands to iron-containing adducts and molecules observed in this work.

Species	Symmetry	Wavenumber / cm^{-1}				Assignment
		Experimental		Calculated		
		This work	Literature	This work DFT (DFT-D)	Literature	
Species observed upon deposition						
Fe:H_2O	^{5}A"	3661	–	3649 (3660)	3802[a]; 3778[b]	ν_{aOH}
		–	–	3547 (3554)	3691[a]; 3656[b]	ν_{sOH}
		1562	1563[c]; 1562[a]	1565 (1567)	1592[a]; 1614[b]	δ_{OH_2}
Fe_2:H_2O	^{7}A'	3739	–	3726 (3731)	–	ν_{aOH}
		3685	–	3632 (3634)	–	ν_{sOH}
		1576	1576[c]	1585 (1586)	–	δ_{OH_2}
Species observed after UV irradiation						
HFeOH	^{5}A"	3742	–	3787	3972[a]; 3963[b]; 3831[d]	ν_{OH}
		1733	1732[c]; 1731[a]	1777	1801[a]; 1871[b]; 1806[d]	ν_{FeH}
		682	682[c]; 680[a]	684	708[a]; 788[b]; 683[d]	ν_{FeO}
		458	458[c]	475	287[a]; 406[b]; 411[d]	$\delta_{FeOH}/\delta_{HFeO}$
HFeOFeH	$^9A_1$	1725[e]/1712	1724/1708[c]; 1708[a]	1778/1767	1771/1447[d]	ν_{FeH}
		914	915/912[c]; 912[a]	849	780/692[d]	ν_{FeO}
$Fe(OH)_2$	^{5}A	3728	–	3774/3773	3939/3938[a]	ν_{OH}
		737	736[c]; 737[a]	745	761[a]	ν_{aFeO}
		631	–	622	631[a]	ν_{sFeO}
		513	–	544/520	439[a]	$\delta_{OFeO}/\delta_{FeOH}$
FeO	$^5\Delta$	873	873[a,f]	923	1008[b]	

[a] From Zhang *et al.*[12] matrix isolation FTIR (Fe atoms produced by laser ablation) and DFT (B3LYP functional) study; [b] From Mebel *et al.*[52] DFT (B3LYP functional) study; [c] From Kauffman *et al.*[11] matrix isolation FTIR study (Fe atoms produced by sublimation); [d] From Gutsev *et al.*[20] DFT study on Fe_nH_2O clusters (BPW91 functional); [e] Very weak band; [f] From Green *et al.*[53] and Chang *et al.*[54] matrix isolation FTIR studies of FeO.

Table 2: Attribution of UV spectral bands to iron and iron-containing adducts (band positions in nm and intensities reported as in the literature).

Species	Free atom		Argon matrix	
	Exp.[a]	Calc. SO-CASPT2[b]	1:1000 (present work)[c]	1:2000 (literature)[d]
	Position(I^2)	Position(Rel. Osc. Str.)	Position(Rel. I)	Position(Osc. Str.(or *I*))
Fe	248.4(4.6) x^5F_5	232.1(0.59) $3d^64s4p\ x^5F_5$		*236.4(52)*
				237.8(88)
	250.2 x^5D_3	241.9(0.11) $3d^64s4p\ x^5D_3$		
	252.4(4.1) x^5D_4	243.7(0.51) $3d^64s4p\ x^5D_4$		*241.4(72)*
			248.5(0.44)	243.9(0.0033)
				246.0(57)
	272.0(4.0) y^5P_3	272.8(0.65) $3d^64s4p\ y^5P_3$		*248.2(59)*
			267.1(0.63)	263.9(0.0033)
				267.4(15)
				269.6(0.0029)
	293.8(5.0) y^5F_4	286.0(0.21) $3d^74p\ y^5F_4$		271.4(0.0003)
				279.0(0.0008)
			287.2(0.77)	286.0(0.0017)
	296.8 y^5F_5	288.7(0.43) $3d^74p\ y^5F_5$		291.1(0.0012)
	298.4 y^5D_3	297.2(0.25) $3d^74p/3d^64s4p\ y^5D_3$		294.5(0.0042)
	302.1 y^5D_4	**300.7(1.00)** $3d^74p/3d^64s4p\ y^5D_4$		*295.5(15)*
				297.7(23)
			296.2(0.79)	299.2(0.0059)
	344.1(6.1) z^5P_3	352.4(0.04) $3d^64s4p\ z^5P_3$		*299.8(38)*
			314.3(0.42)	301.0(0.0005)
				306.9(4)
			326.6(0.52)	325.8 (0.0006)
			337.4(0.56)	337.1(0.0003)
	372.1 z^5F_5	378.5(0.07) $3d^64s4p\ z^5F_5$	352.1(0.75)	351.9(0.0008)
	382.6(6.0) z^5D_3	389.0(0.01) $3d^64s4p\ z^5D_3$	364.8(1.00)	363.9(0.0004)
	386.1 z^5D_4	392.1(0.03) $3d^64s4p\ z^5D_4$	378.4(0.76)	378.0(0.0007)
Fe_2	–	–	414	415
	–	–	468	474
Fe:H_2O	–		387(0.08)	–
	–	380.9(0.42) $3d^64s4p(0.51)/\ 3d^74p(0.32)$	372(0.28)	–
	–	363.8(0.37) $3d^64s4p(0.17)/\ 3d^74p(0.62)$	356(0.27)	–
	–	350.2(0.49) $3d^64s4p(0.17)/\ 3d^74p(0.62)$	342(0.74)	–
	–	348.4(0.14) $3d^64s4p(0.17)/\ 3d^74p(0.62)$		–
	–	342.9(0.53) $3d^64s4p(0.14)/\ 3d^74p(0.59)$		–
	–	342.2(0.55) $3d^64s4p(0.10)/\ 3d^74p(0.67)$		–
	–	340.8(0.14) $3d^64s4p(0.10)/\ 3d^74p(0.58)$	331(0.94)	–
	–	333.5(0.14) $3d^64s4p(0.17)/\ 3d^74p(0.53)$	324(1.00)	–
	–	329.9(0.32) $3d^64s4p(0.26)/\ 3d^74p(0.48)$	320(0.99)	–
	–	329.8(0.16) $3d^64s4p(0.28)/\ 3d^74p(0.45)$		–
	–	305.1(0.74) $3d^64s4p(0.26)/\ 3d^74p(0.48)$	297(0.65)	–
	–	305.1(0.17) $3d^64s4p(0.26)/\ 3d^74p(0.49)$		–
	–	296.4(0.38) $3d^64s4p(0.56)/\ 3d^74p(0.14)$	281(0.76)	–
	–	296.4(0.39) $3d^64s4p(0.56)/\ 3d^74p(0.14)$		–
	–	290.8(0.46) $3d^64s4p(0.57)/\ 3d^74p(0.09)$		–
	–	290.8(0.24) $3d^64s4p(0.57)/\ 3d^74p(0.09)$		–
	–	290.2(0.18) $3d^64s4p(0.56)/\ 3d^74p(0.09)$		–
	–	280.6(0.97) $3d^64s4p(0.59)/\ 3d^74p(0.08)$	270(0.45)	–
	–	**280.6(1.00)** $3d^64s4p(0.59)/\ 3d^74p(0.08)$		–
Fe_2:H_2O	–		430	–
	–		451	–

[a] Experimental reference data for free Fe atom from Nave *et al.*;[55] [b] SO-CASPT2 energy levels for free iron atoms and SO-MS-CASPT2 energy levels for Fe:H_2O adducts, with relative oscillator strengths in parentheses; [c] Positions of absorption bands in experimental spectra presented in this work (Fe:Ar ∼1:1000), with relative abundance in parentheses; [d] Experimental reference data for Fe in an argon matrix (Fe:Ar 1:2000) from Mann & Broida,[56] with oscillator strengths in parentheses and poorly resolved bands in italics (with intensities rather than oscillator strengths). Experimental reference data for Fe_2 in an argon matrix from de Vore *et al.*[57]

Table 3: Attribution of IR spectral bands to iron-containing adducts and molecules observed for deuterated water.

Species	Wavenumber / cm^{-1}			
	Experimental		Calculated	
	This work[a]	Literature	This work DFT (DFT-D)	Literature
Species observed upon deposition				
D_2O	2772, 2658, 1176	2772, 2658, 1176[b]	2789, 2671, 1180	2875, 2754, 1200[f]
Fe:D_2O	2675, –, 1159	–, –, 1158[c,d]	2673, 2555, 1145 (2681, 2560, 1146)	–
Fe_2:D_2O	2716, –, 1169	–, –, 1169[d]	2729, 2617, 1160 (^{7}A') (2736, 2619, 1161)	–
			2728, 2601, 1151, 1158 (^{9}A)	–
Species observed after UV irradiation				
DFeOD	–, 1246, 675/670, –	–, 1246/1245, 660/661, –[c,d]	2758, 1267, 668, 362	–
FeO	873	873[c]	923	1008[e]

[a] Where no value is given, the experimental band was either too weak to be observed under our experimental conditions, or, in the case of DFeOD, was too close to the ν_2 of CO_2 to be extracted; [b] From Bentwood *et al.*[60] matrix isolation FTIR study; [c] From Zhang *et al.*[12] matrix isolation FTIR and DFT (B3LYP functional) study; [d] From Kauffman *et al.*[11] matrix isolation FTIR study; [e] From Mebel *et al.*;[52] [f] From Coussan *et al.*[61]

Table 4: Energetics for the formation of Fe:H_2O adducts and photoproducts determined at the BPW91/cc-pVTZ (DFT) and at the CCSD(T)/cc-pVTZ//DFT levels of theory. ZPEs are computed at the DFT level. Regarding the complexes with the Fe dimer, the energetics were determined with respect to the ground-states of Fe_2 at the DFT and CCSD(T) level, that is to say $^7\Delta_u$ and $^9\Sigma_g^-$ respectively (see text).

Reactants	Products	ΔH(0K) / kJ mol^{-1}	
		DFT (DFT-D)	CCSD(T)//DFT (//DFT-D)
Fe + H_2O	Fe(H_2O) (^{5}A")	-39 (-44)	-16 (-13)
	HFeOH (^{5}A")	-159	-129
	FeO ($^5\Delta$) + H_2	-29	+113
Fe + 2 H_2O	(H_2O)Fe(H_2O) (^{3}A)	-62 (-70)	+27 (+32)
	(H_2O)Fe(H_2O) (^{5}A)	-55 (-65)	-3.5 (-9)
	Fe(H_2O)$_2$ (^{5}A)	-74 (-89)	-52 (-44)
	HOFeOH (^{5}A) + H_2	-266	-225
Fe_2 + H_2O	Fe_2(H_2O) (^{7}A')	-47 (-54)	+14 (+18)
	Fe_2(H_2O) (^{9}A)	+12 (+3)	-26 (-0.1)
	HFe_2OH (^{7}A)	-155	-101
	HFe_2OH (^{9}A)	-104	-133
2 Fe + H_2O	HFeOFeH ($^9A_1$)	-333	-288

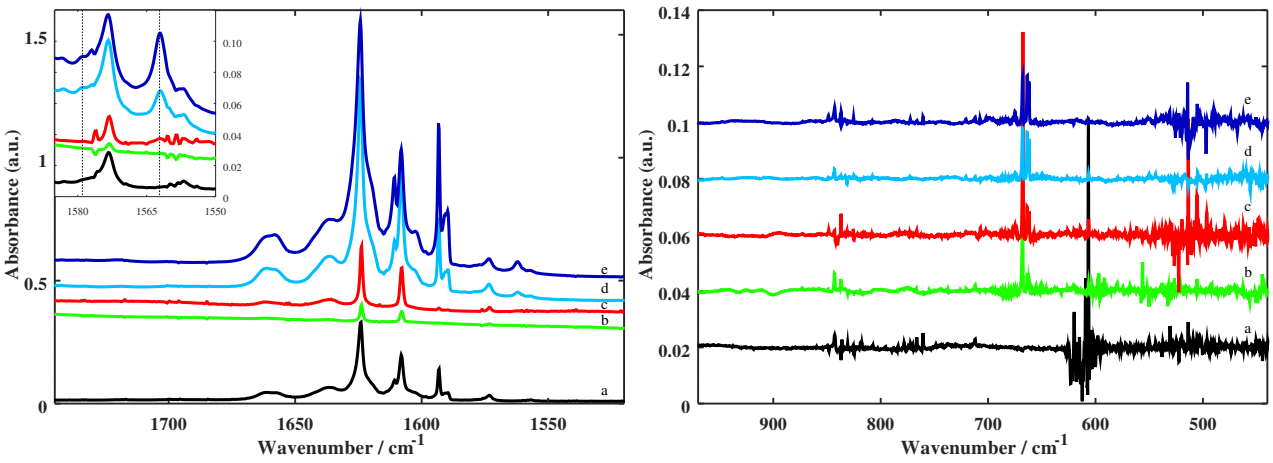

Figure 1: Depositions of Fe:H_2O:Ar with increasing H_2O concentrations in the spectral regions 1745 – 1520 cm^{-1} (left hand panel) and 970 – 400 cm^{-1} (right hand panel). Individual spectra are as follows: a) H_2O:Ar (reference) from a gas phase mixture of $\sim$ 1:200, b) - e) depositions of Fe:H_2O:Ar with increasing concentrations of H_2O. In the 1745 – 1520 cm^{-1} (left hand panel) spectral region, water aggregates give rise to a series of absorption features, as observed in spectrum a, including the peaks at 1573 and 1557 cm^{-1} in the inset, which are attributed to ν_2 bending vibrations.[58] The inset highlights the presence of bands attributed to Fe:H_2O (1562 cm^{-1}) and Fe_2:H_2O (1579 cm^{-1}). The latter is only visible for higher H_2O concentrations. In the 970 – 400 cm^{-1} spectral region (right hand panel), as expected there are very few bands, all of which are attributable to the presence of trace amounts of contaminents in the matrix (for example, CO_2 at $\sim$ 670 cm^{-1}) or detector noise.

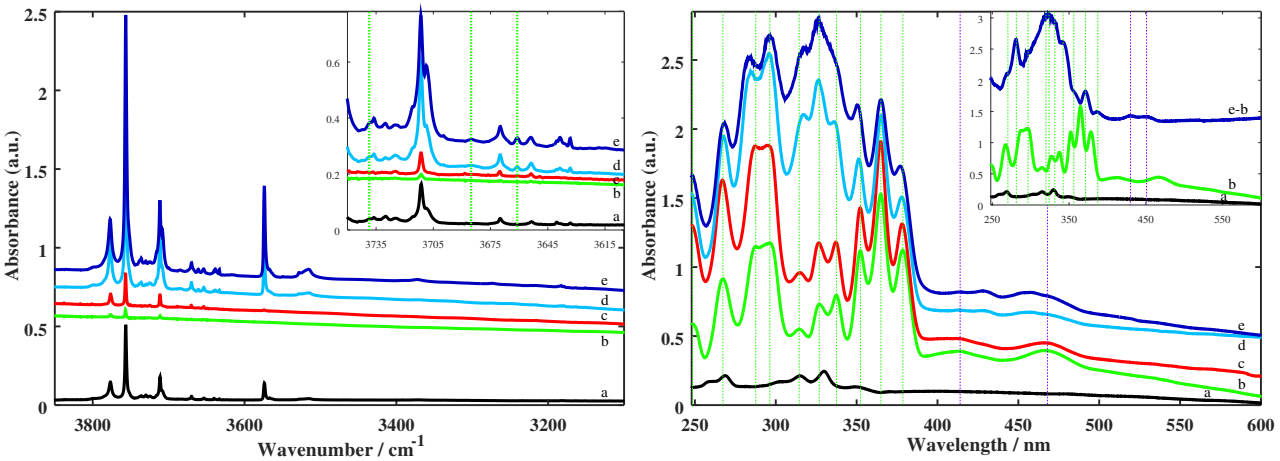

Figure 2: Depositions of Fe:H_2O:Ar with increasing H_2O concentrations in the spectral regions 3850 – 3100 cm^{-1} (left hand panel) and 245 – 600 nm (right hand panel). Individual spectra are as follows: a) H_2O:Ar (reference) from a gas phase mixture of $\sim$ 1:200, b) – e) depositions of Fe:H_2O:Ar with increasing concentrations of H_2O. In the left hand panel inset, bands attributed to Fe:H_2O and Fe_2:H_2O adducts are highlighted with dotted lines at 3661 (Fe:H_2O), 3685 (Fe_2:H_2O), and 3739 (Fe_2:H_2O) cm^{-1}. In the right hand panel, peaks attributed to Fe are highlighted with green dotted lines (249 – 378 nm) while those attributed to Fe_2 are identified in purple (414 and 468 nm). The inset replots spectra a and b, and compares them to the difference spectrum e-b, i.e. the difference between the spectrum of Fe:H_2O:Ar and that of Fe:Ar, in order to highlight the bands attributed to the Fe:H_2O adduct. Overplotted in green are peaks attributed to Fe:H_2O adducts (270 – 387 nm) and in purple to Fe_2:H_2O (430, 451 nm).

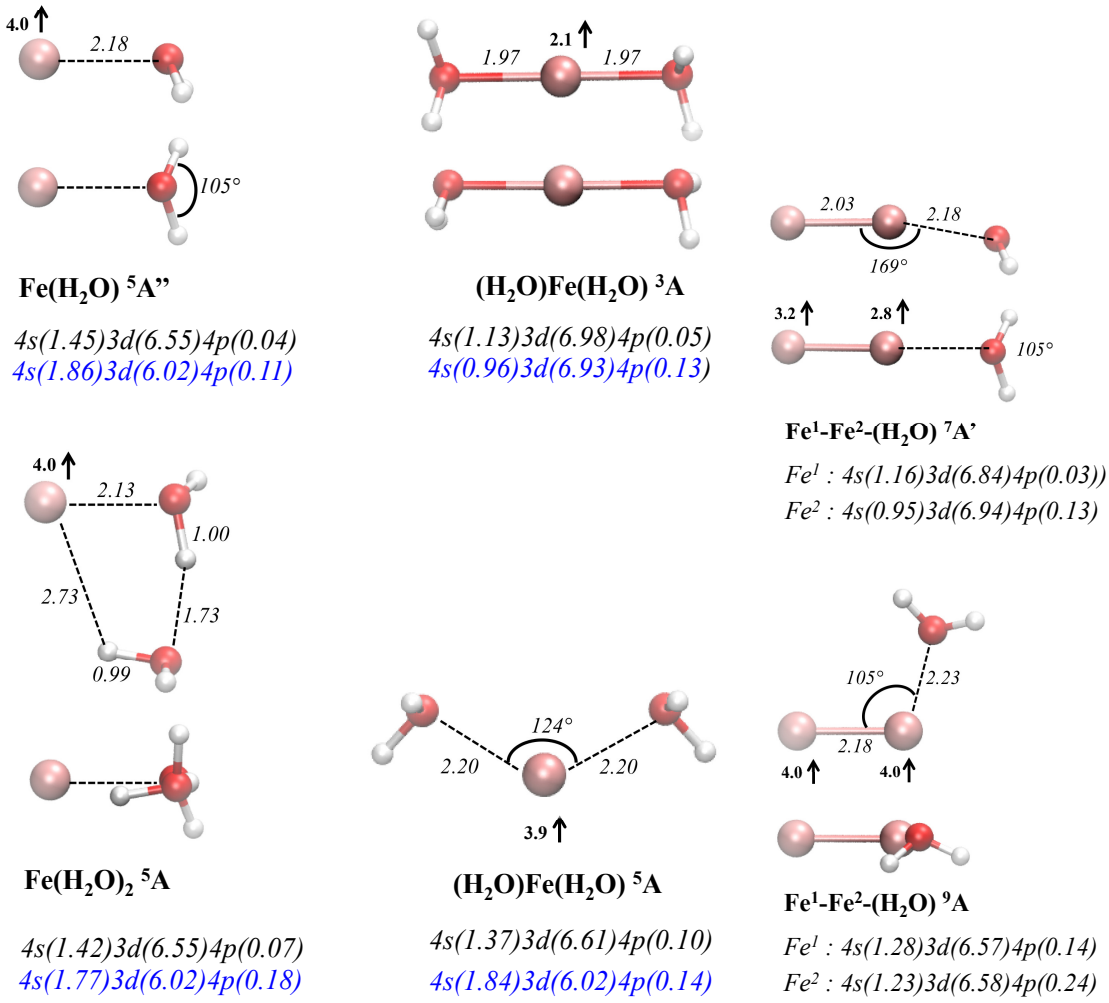

Figure 3: BPW91/cc-pVTZ optimised geometries of iron-water complexes (two views are shown when necessary for clarity). The stoichiometries and electronic states are specified in bold characters, along with the natural population on the valence orbitals of the Fe atoms (in italics, in black: DFT, in blue: CCSD(T)//DFT). When larger than 0.1, the spin densities are mentioned. Relevant bond/intermolecular distances (in angstroms) and angles (in degrees) are also reported.

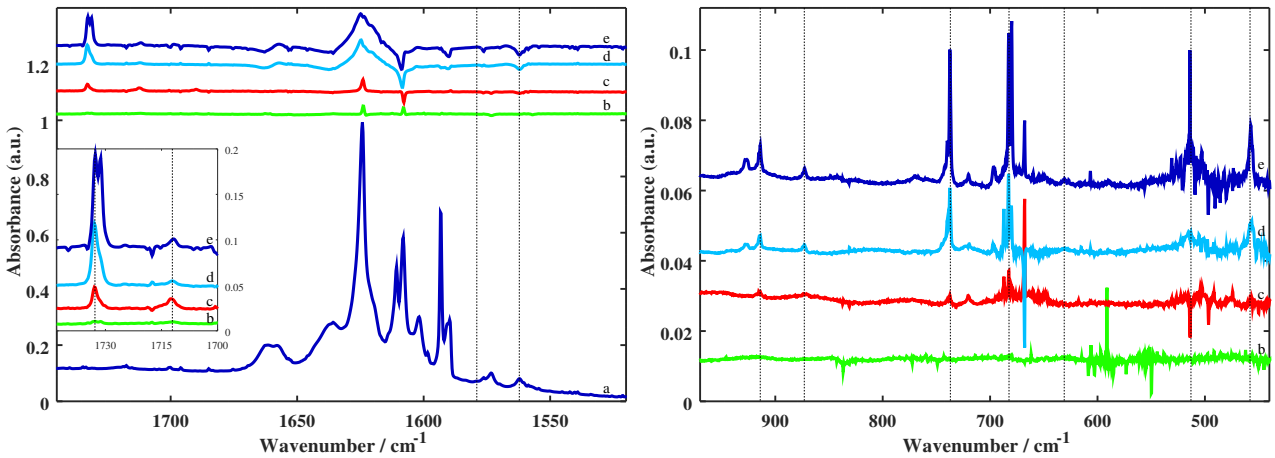

Figure 4: Processing of Fe:H_2O:Ar matrices with UV radiation ($\lambda < 235$ nm), presented in the spectral regions 1745 – 1520 cm^{-1} (left hand panel) and 970 – 400 cm^{-1} (right hand panel). In the left hand panel, spectrum a is an unprocessed Fe:H_2O:Ar matrix (spectrum e in Fig 1), presented for comparison to the processed spectra. The spectra b–e are presented as difference spectra (irradiated minus non-irradiated samples) for increasing concentrations of H_2O. Dotted lines represent the position of Fe:H_2O and Fe_2:H_2O complexes (1562 and 1579 cm^{-1}), which decrease upon irradiation. The inset presents a zoom of the 1700–1740 cm^{-1} region, where, upon irradiation, new bands are formed at 1733 and 1712 cm^{-1}. These are attributed to the insertion of Fe and Fe_2 into H_2O, as has previously been reported in the literature. In the right hand panel, four spectra (traces b–e) are presented. These spectra, corresponding to the difference spectra of the four Fe:H_2O:Ar matrices after processing with UV radiation, have the same labels as those in the left hand panel and in Figure 1. Various photoproduct absorption bands appear upon irradiation, and their attributions are detailed in Table 1 and in the text.

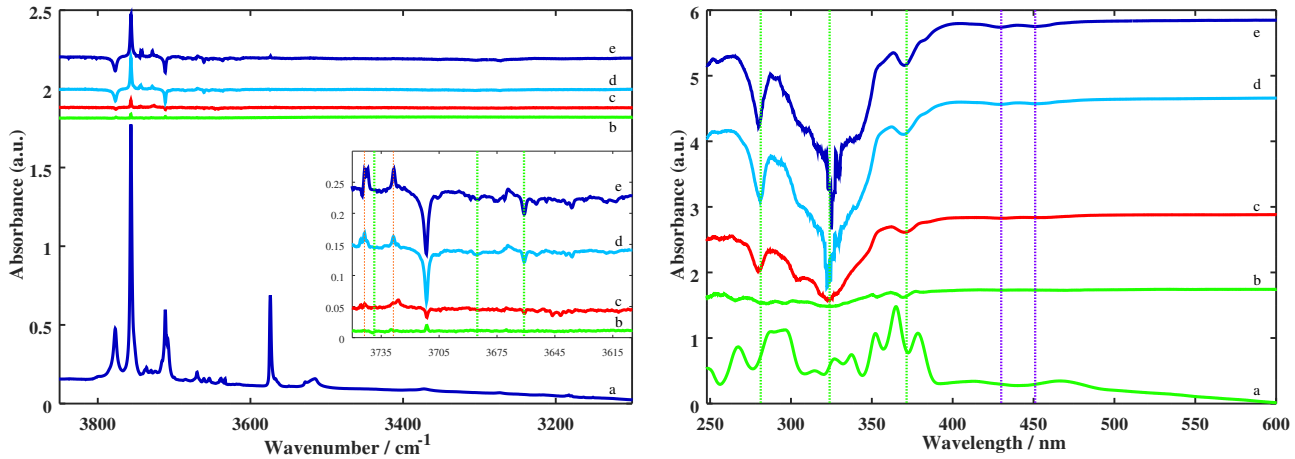

Figure 5: Processing of Fe:H_2O:Ar matrices with UV radiation ($\lambda < 235$ nm), presented in the spectral regions 3850 – 3100 cm^{-1} (left hand panel) and 245 – 600 nm (right hand panel). In the left hand panel, spectrum a is an unprocessed Fe:H_2O:Ar matrix (spectrum e in Fig 1), presented for comparison to the processed spectra. The spectra b–e are presented as difference spectra (irradiated minus non-irradiated samples) for increasing concentrations of H_2O. The inset presents a zoom of the 3750–3610 cm^{-1} region, where, upon irradiation, bands attributed to Fe:H_2O and Fe_2:H_2O decrease while new bands appear at 3742 and 3728 cm^{-1}. By comparison with calculations, these are attributed to the insertion of Fe into H_2O and to the formation of $Fe(OH)_2$. In the right hand panel, spectrum a is an unprocessed Fe:H_2O:Ar matrix with only a trace of H_2O (spectrum b in the right hand panel of Figure 2) for comparison with the processed spectra b –e. Bands corresponding to Fe:H_2O and Fe_2:H_2O adducts disappear with irradiation (the three most intense for Fe:H_2O (281, 324, 372 nm) and the two bands for Fe_2:H_2O (430, 451 nm) are plotted here to guide the eye).

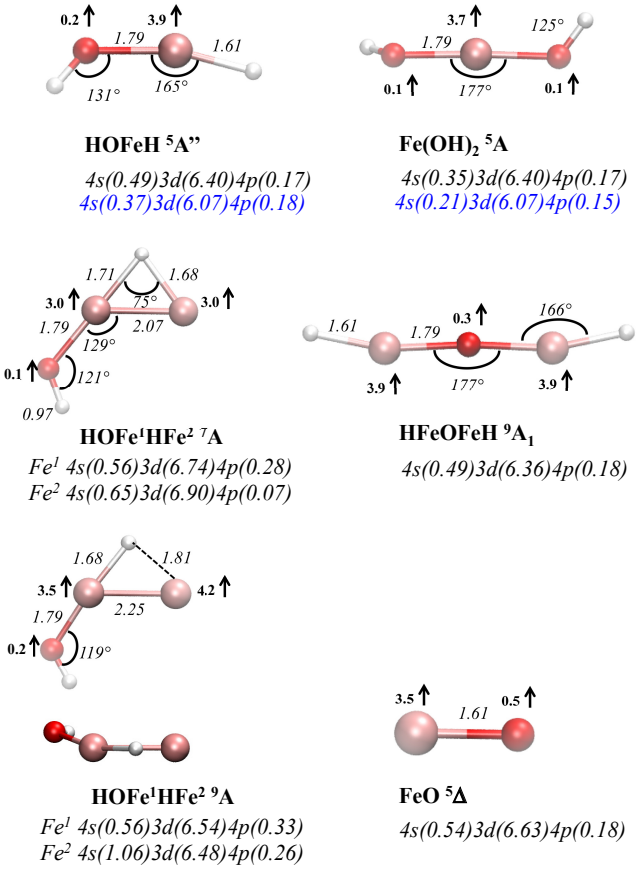

Figure 6: As for Figure 3, BPW91/cc-pVTZ optimised geometries of iron-water complex photoproducts.

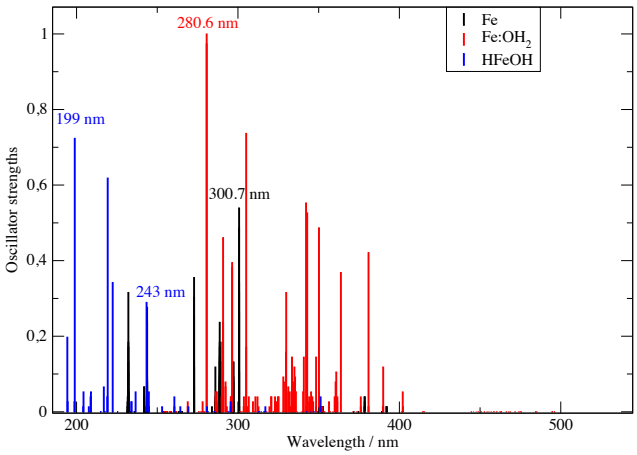

Figure 7: The calculated electronic spectra of Fe, Fe:OH_2 and HFeOH. The oscillator strengths are all relative to the maximal value obtained for the Fe:OH_2 complex.

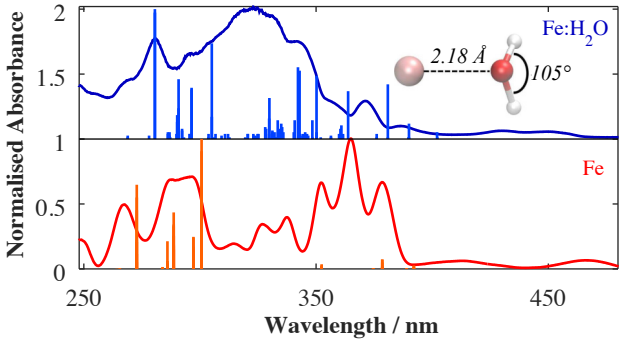

Figure 8: Graphical ToC entry.